The Influence of Shrinkage-Reducing Admixtures (SRAs) on Moisture Absorption in Cementitious Materials at Early-Ages

Gaurav Sant[*], *Arnd Eberhardt*[†], *Dale Bentz*[‡] *and Jason Weiss*[§]

1.0. Abstract

The water absorption behavior of cement pastes (*w/c* = 0.30) containing varying concentrations (i.e., 0 %, 0.2 % and 5 %) of a shrinkage reducing admixture (SRA) was measured. Moisture ingress was monitored using x-ray absorption. A decrease in both the depth of water penetration and the rate of water absorption was observed with increasing specimen maturity and admixture concentration. This agrees with theoretical considerations that suggest water sorption is a function of the surface tension and the viscosity of the fluid ingressing into the pores. The Boltzmann-Matano approach was successfully employed to determine the moisture content dependent moisture diffusivity of the material, which exhibited a dependence on both the pore structure (specimen maturity) and the admixture concentration.

Keywords: shrinkage reducing admixture (SRA), water absorption, moisture transport, moisture diffusivity, sorption, early-age, x-ray absorption

[*] Research Assistant (Corresponding Author), Purdue University, School of Civil Engineering, Materials Sensing and Characterization Laboratory, 550 Stadium Mall Drive, West Lafayette, IN 47907, USA, Phone: +1-765-494-0358, Fax: +1-765-494-0395, Email: gsant@purdue.edu
[†] Research Assistant, Swiss Federal Institute for Materials Testing and Research (EMPA), Laboratory for Concrete and Construction Chemistry, Überlandstrasse 129, CH-8600 Dübendorf, Switzerland, Phone: +41-44-823-4193, Fax: +41-44-823-4035, Email: Arnd.Eberhardt@empa.ch
[‡] Chemical Engineer, Building and Fire Research Laboratory, National Institute of Standards and Technology, 100 Bureau Drive, Stop 8615, Gaithersburg, MD 20899, USA, Phone: +1-301-975-5865, E-mail: dale.bentz@nist.gov
[§] Professor and Associate Head, Purdue University, School of Civil Engineering, 550 Stadium Mall Drive, West Lafayette, IN 47907, USA, Phone: +1-765-494-0358, Fax: +1-765-494-0395, Email: wjweiss@purdue.edu

2.0. Introduction and Background

Shrinkage reducing admixtures (SRAs) are being increasingly used in concrete construction [1]. Shrinkage reducing admixtures work by reducing the surface tension of the pore fluid which in turn reduces the capillary stress developed and the shrinkage of concrete [2,3]. Several studies have demonstrated that SRAs can substantially reduce shrinkage (both, drying and autogenous) while having a minimal impact on mechanical properties such as strength or elastic modulus [4,5,6,30]. Several researchers have shown that reducing shrinkage results in a reduction or elimination of cracking in concrete elements [7,8,9,10].

While the majority of research has focused on assessing the influence of shrinkage reducing admixtures on volume change, the impact of these admixtures on material durability has received less attention [4,30,31,33,34,41,47]. Schissel et al. assessed the rapid chloride penetrability of concrete mixtures containing SRA and observed them to provide a greater resistance to ionic transport than conventional mixtures [11]. This may be due in part to the reduction in the conductivity of the solution containing SRA [45]. Further, Bentz et al. [43] demonstrated that additions of SRA may reduce the diffusion rate of ionic species due to the increase in the viscosity of the pore solution. Berke et al. [12] have shown that reinforced concrete containing a shrinkage reducing admixture may also have a lower potential for corrosion related damage and deterioration as compared to reinforced concrete not containing such an admixture.

Other researchers have investigated the influence of SRA on the freeze-thaw resistance of concrete. While some have suggested that the SRA may in some cases interact with the air

entraining admixture resulting in a reduction in the stability of the air system [13,14] or reduce the scaling performance under freeze-thaw loading [15], others have shown that it is possible to make concretes with a sufficient air void system [17]. It has often been anecdotally observed that concrete containing SRA can be even more resistant to freezing and thawing than conventional concrete after some drying is permitted [16,17]. This can be explained by observations that water is absorbed less quickly into concrete containing SRA [1,47]. This has been attributed to the reduction in surface tension of the pore fluid.

A need exists for the development of more comprehensive approaches for quantifying the water absorption behavior of concretes containing SRA. This has implications on the interpretation of laboratory tests like chemical shrinkage, chloride ingress or freeze thaw testing and can also have a substantial impact on the field performance and service life modeling of concrete containing SRA. Specifically, this could include water absorption during curing, saturation leading to freeze thaw damage, or the ingress of aggressive ionic agents.

3.0. Research Significance

This paper quantifies how SRAs reduce water absorption and relates this to a moisture diffusivity coefficient. The diffusivity coefficient is related to considerations of specimen age (maturity), and surface tension and the viscosity of the pore fluid. These results demonstrate a benefit of SRAs in reducing moisture ingress and enable this effect to be incorporated from a fundamental perspective in service life models which aim to predict the durability performance of structures.

4.0. Materials and Mixing Procedures

Three cement paste mixtures were prepared according to the mixture proportions shown in Table 1. Type I ordinary portland cement was used. The cement had a Blaine fineness of 360 m^2/kg and a Bogue potential phase composition (mass fraction) of 60 % C_3S, 12 % C_2S, 12 % C_3A, and 7 % C_4AF, with a Na_2O equivalent of 0.72 %. A high-range water reducing admixture (HRWRA - Glenium 3000NS©[**]) was used. A commercially available shrinkage reducing admixture (SRA - Tetraguard AS20©) was added at 0.2 % and 5 % concentration (based on the initial water to SRA replacement rates by mass) of the initial mixing water. The mixture compositions (SRA concentrations) were specifically selected to evaluate the moisture transport performance of mixtures having three distinct values of liquid-vapor surface tensions (72 x 10^{-3} N/m, 54 x 10^{-3} N/m, and 38 x 10^{-3} N/m) (Further details are provided in Sections 6.2 and 7.2).

A mixing procedure was used in preparation of the cement pastes that permitted mixing to be performed under an evacuated condition, to minimize the influence of entrapped air on the measurements. The cement paste mixtures were prepared using de-aired, de-ionized water. The water was de-aired by boiling and then cooled to room temperature (23 ± 1) °C before mixing. The dry constituent materials were placed in a special mixing chamber [18,19]. The chamber was sealed, air was evacuated from the chamber using a vacuum pump, and the solution of water and the chemical admixtures was introduced into the chamber under the same evacuated condition. The chamber was then placed in a commercial paint shaker and shaken for 5 min to mix the

[**] Certain commercial products are identified in this paper to specify the materials used and procedures employed. In no case does such identification imply endorsement by Purdue University or the National Institute of Standards and Technology, nor does it indicate that the products are necessarily the best available for the purpose.

89 constituents and obtain a consistent paste mixture. After mixing, the chamber was opened and
90 the cement paste slurry was placed in the specimen molds using external vibration [19].
91
92 **Table 1: Mixture Proportions (by Mass)**
93

	w/c = 0.30	*w/c* = 0.30 + 0.2 % SRA	*w/c* = 0.30 + 5 % SRA
Water	0.3000	0.2994	0.2850
Cement	1.0000	1.0000	1.0000
HRWRA	0.0050	0.0050	0.0050
SRA	0.0000	0.0006	0.0150

94

95 **5.0. General Information on the X-Ray Absorption Facility**
96
97 The equipment used is an x-ray absorption system produced by GNI [20]. The system consists of
98 a modified Type 9120 x-ray source (tube) contained in an environmentally controlled
99 (temperature and humidity) chamber [21]. For the x-ray energy settings (Power = 2.5 W; 50 KeV
100 and 50 μA) used in this study, the spot size of the source was approximately 0.0055 mm [21]. The
101 x-ray beam output by the source exhibits a conical spread [21].
102
103 The x-ray intensity was measured using a charge-coupled device (CCD) (i.e., x-ray camera). The
104 16-bit CCD camera records the cumulative x-ray intensity at each pixel, for a total surface of
105 252 pixels x 256 pixels [22]. The x-ray source and camera can be moved simultaneously using an
106 X-Y positioning table with a precision of ± 0.001 mm. The Focus to Detector Distance (FDD,
107 Figure 1), can be adjusted from 10 mm to 500 mm; however, for this study the FDD was fixed at
108 500 mm. The Object to Detector Distance (ODD) was fixed at 100 mm for this study (Figure 1).
109

The specimens analyzed in this study are mounted on a fixed stage, which allows the user to perform repetitive imaging, ensuring a fixed specimen position. An illustration of the experimental setup is provided in Figure 1. A single pixel size and spatial resolution (refer section 5.2) of 0.08 mm has been determined for the geometry used in this investigation.

A critical consideration in moisture movement studies is the need to resolve the spatial position and moisture content of the specimen. Spatial resolution is crucial to identify the position of the moisture front in the system. Further, it may also be important to account for mismatch of the attenuation coefficients and the consequent loss in spatial resolution which is encountered at the specimen-air interface [23]. These considerations will be discussed further in Section 5.2.

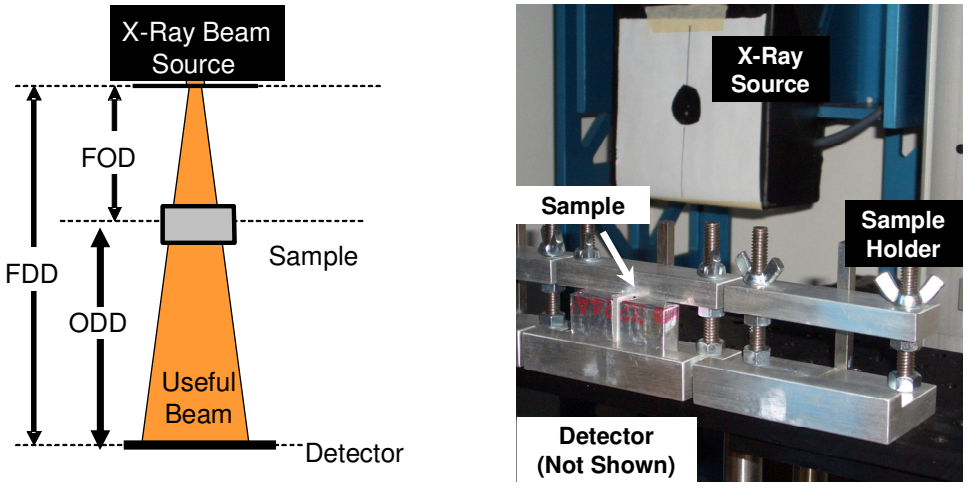

(a) *(b)*

Figure 1: Equipment Layout: (a) A schematic illustration of the geometry of the experimental setup (not to scale) and (b) A photo of the specimen in the x-ray chamber

127 **5.1. Analytical Assessment of Moisture Movement using X-Ray Absorption**

128

129 The intensity of x-ray radiation transmitted at any time through a dry element can be described
130 using Equation 1, while Equation 2 describes the intensity of radiation transmitted through the
131 same element that contains moisture [24].

132 $$I_{DRY} = I_0 \cdot \exp\left[-\left(\mu_{Eff}\right) \cdot t\right] \qquad \text{Equation (1)}$$

133 $$I_{WET} = I_0 \cdot \exp\left[-\left(\mu_{Eff.} \cdot t + \mu_W \cdot t_W\right)\right] \qquad \text{Equation (2)}$$

134 where: μ_{Eff} and t are the effective linear attenuation coefficient and thickness of the dry volume
135 element and μ_W and t_W are the linear attenuation coefficient and the thickness of the volume of
136 water present in the material [25].

137

138 To describe the influence of moisture ingress on the transmitted x-ray behavior, the ratio of the
139 wet and dry transmitted intensities can be compared. This can be done by rearranging and
140 reducing Equation 1 and Equation 2. This expression is shown in Equation 3.

141 $$\frac{I_{WET}}{I_{DRY}} = \exp\left[-\mu_W \cdot t_W\right] \qquad \text{Equation (3)}$$

142 The moisture content (MC) of a porous specimen (m^3/m^3) can be expressed as a ratio of the
143 volume of water (m^3) absorbed to total (solid) volume of the dry material (m^3). This can be
144 written as shown in Equation 4 where V_i is the volume fraction of water (moisture content)
145 contained in the specimen.

146 $$MC = V_i = \frac{t_W}{t} \qquad \text{Equation (4)}$$

147 Equations 3 and 4 can then be rearranged to represent the moisture that exists in the material
148 (described in Equation 5) as a function of the logarithm of the ratio of the transmitted intensities
149 in the wet and the dry states, the attenuation coefficient of water (at a specified energy level) and
150 the thickness of the material in the dry state [25].

151 $$MC = \frac{\ln\left(\frac{I_{WET}}{I_{DRY}}\right)}{\left(-\mu_W \cdot t\right)} \qquad \text{Equation (5)}$$

152

153 **5.2. Spatial and Moisture Content Resolution of the X-Ray Absorption Facility**

154

155 Figure 2(a) shows the spatial resolution as a function of magnification (Equation 6) [26,27].

156 $$R_w = \frac{S_P}{M} + \left(1 - \frac{1}{M}\right) \cdot S_S + \frac{(M-1) \cdot t \cdot \sqrt{x^2 + y^2}}{ODD} \qquad \text{Equation (6)}$$

157 where S_P is the single-pixel size on the camera (0.08 mm in this study), M (M = 1 + ODD/FOD)
158 is the level of magnification (1.25X in this study), S_S is the spot-size of the x-ray beam at the
159 source (0.0055 mm), t is the specimen thickness (12.7 mm in this study) and x and y are the
160 dimensions from the center of the specimen to its visible edges in the horizontal and vertical
161 directions (mm). Figure 2(a) illustrates that increasing the magnification increases the spatial
162 resolution (increasing values denote a loss in resolution). For the setup used in this study and a
163 specimen thickness of 12.7 mm, a spatial resolution of ≈0.08 mm to ≈0.39 mm was determined,
164 at the center and visible edges of the specimen respectively.

165

166 The moisture content resolution (%) of the x-ray facility for the present experiments can be
167 described by ascertaining the coefficient of variation (COV) of the transmitted intensity for a dry

specimen (or a specimen containing a specific fixed level of moisture). Multiple measurements (3) on a single specimen tested in the dry state demonstrate a measurement (intensity) variability (COV) of 0.55 %. Using the ratio of the transmitted intensity of a wet specimen (containing a variable level of moisture), the transmitted intensity of a dry specimen, the effective attenuation coefficient of water at a specific energy level (cm^{-1}), and the thickness of the specimen (cm), the relationship between the normalized x-ray intensity and the moisture content can be determined (Equation 5). This relationship is graphically illustrated in Figure 2(b) [25].

For an incident beam power of 2.5 W (50 KeV and 50 μA), a coefficient of variation of 0.55 % in the transmitted intensity was determined for a dry paste specimen [25].While the attenuation coefficient of water shows maximum sensitivity at low beam energies, practical considerations of beam energy and variability justify selection of 50 KeV as an appropriate imaging energy, as a trade-off is needed between low variability and a decreasing sensitivity for the attenuation due to water [25]. The volumetric moisture content resolution is then determined to be 0.0055 (m^3/m^3) which for the material tested (cement paste, bulk density of 2100 kg/m^3) is equivalent to a mass-based moisture content resolution of 0.26 % (kg/kg). The moisture resolution is shown graphically in Figure 2(b).

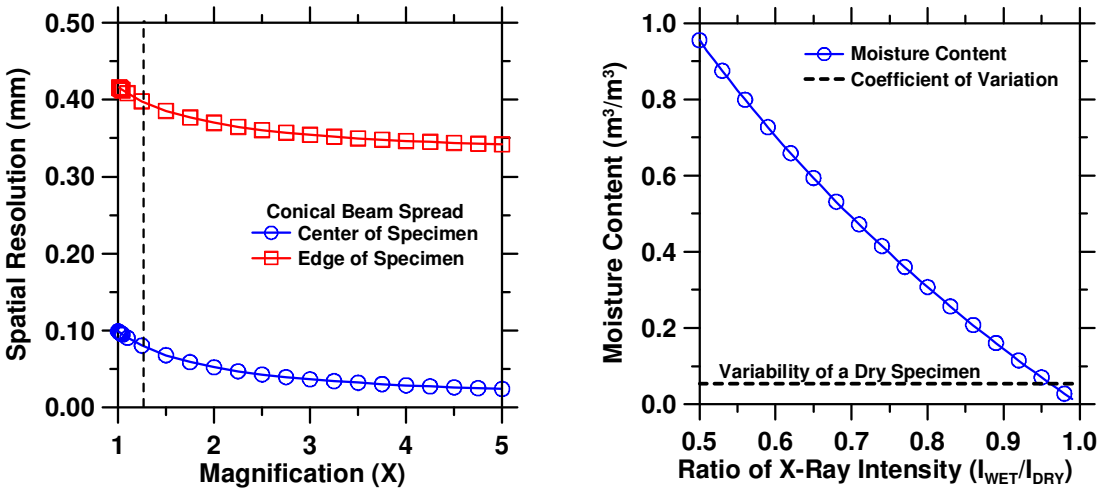

(a) *(b)*

Figure 2: (a) Spatial resolution as a function of magnification at the center of the specimen. The dashed line indicates the magnification level used in this study and (b) The moisture content as a function of the normalized x-ray intensity and the minimum moisture resolution (dashed line)

6.0. Experimental Procedures

6.1. Fluid Surface Tension and Viscosity Measurements

The surface tensions of solutions of SRA and de-ionized (DI) water and SRA and synthetic pore solution (0.35 KOH + 0.05 NaOH – molar concentration) were measured using the du Noüy Ring Method at 23 ± 0.5 °C [28]. The method is based on determining the force that is required to detach a wire ring from the surface of a solution. The ring used was made of a platinum-iridium alloy and was cleaned according to ASTM D971 prior to each measurement. The measured surface tension of distilled water (0.0723 N/m) was used as a standard reference in determining the change in surface tension caused by the addition of the SRA [29]. The average of three

measurements was used in the representation of each data-point, with a typical coefficient of variation being 0.50 %. A more detailed procedure on performance of the surface tension measurements can be found elsewhere [44,45].

The viscosities of solutions of SRA and de-ionized (DI) water were measured using a Hydramotion 700** portable viscometer, at a temperature of 23 ± 0.5 °C, with an uncertainty of 0.02 mPa·s. The measured viscosity of distilled water (0.89 mPa·s) is used as a standard reference in determining the change in viscosity effected by addition of the SRA. Measurements were performed at a water-SRA mass concentration of 0 %, 0.2 %, 5 % and 10 %.

6.2. Moisture Ingress Assessment Using X-Ray Absorption

Cement paste samples (25.4 mm x 25.4 mm x 12.7 mm, density = 2100 kg/m^3) were used to measure water absorption. A dimensional tolerance of ± 0.5 mm was noted between samples. At degrees of hydration (evaluated using chemical shrinkage measurements [19,30,31,32]) of approximately 10 % and 47 % (equivalent ages of 8 h and 24 h for the plain mixture; *w/c* = 0.30) the samples were demolded and weighed. At this time, the samples were placed in an oven at 50 °C for 2 d to remove the evaporable water contained in the sample, while minimizing the influence of drying on the pore structure. After 2 days of drying, the samples were weighed and the evaporable water content was measured (~30 % and ~20 % for the specimens at 10 % and 47 % hydration respectively on a volumetric basis of the sealed samples). The initial water content of the plain cement paste (*w/c* = 0.30) is ~48 % by volume.

225 At the time of testing, the oven-dried samples were wrapped in two uniform layers of aluminum
226 tape to seal the sample and enable one-dimensional water absorption. Consequently, the
227 measured intensity of x-ray radiation transmitted through the overall specimen would be a
228 function of the thickness of the cement paste and the aluminum tape. After the samples were
229 sealed, they were exposed to x-rays having an energy of 2.5W (50 KeV and 50 μA), for a camera
230 integration (exposure) time of 5 seconds per image. Multiple (3 imaging cycles, which acquired
231 10 images each for a total of 30 images) x-ray images were acquired for the dry samples, to
232 develop a baseline calibration profile in the dry state. This profile was then used to track the
233 time-dependent ingress of moisture into the samples using Equation (5), assuming a uniform
234 moisture front and degree of hydration (reaction) through the specimen volume [25,64]. After
235 testing of the dry samples was completed, water was ponded on the top of the cement paste
236 samples. X-ray measurements were then performed periodically over a duration of 1 hour after
237 water addition to monitor moisture ingress.
238
239 **7.0. Experimental Results**
240 **7.1. Fluid Surface Tension and Viscosity Measurements**
241
242 Figure 3(a) shows the measured surface tension for the DI-Water solutions and synthetic pore
243 solutions (0.35 KOH with 0.05 NaOH – molar concentration) containing various concentrations
244 of a shrinkage reducing admixture (SRA). As observed in Figure 3, dramatic reductions in
245 surface tension are noted even at very low rates of admixture addition. However, a plateau in the
246 reduction in surface tension is achieved when the SRA concentration reaches a critical level of
247 ≈10 % to 15 % [33,34,35]. A similar response is noted for SRA addition in pore solution; however,

the plateau in surface tension reduction is reached at a lower SRA concentration due to the presence and continued dissolution of salts in the pore solution [34,35].

Figure 3(b) shows the measured viscosity of solutions containing various concentrations of an SRA normalized to the viscosity of DI-Water. As observed in Figure 3(b), the solution viscosity increases linearly with increasing SRA concentration, and is ≈55 % higher than DI-Water at an SRA concentration of 10 %.

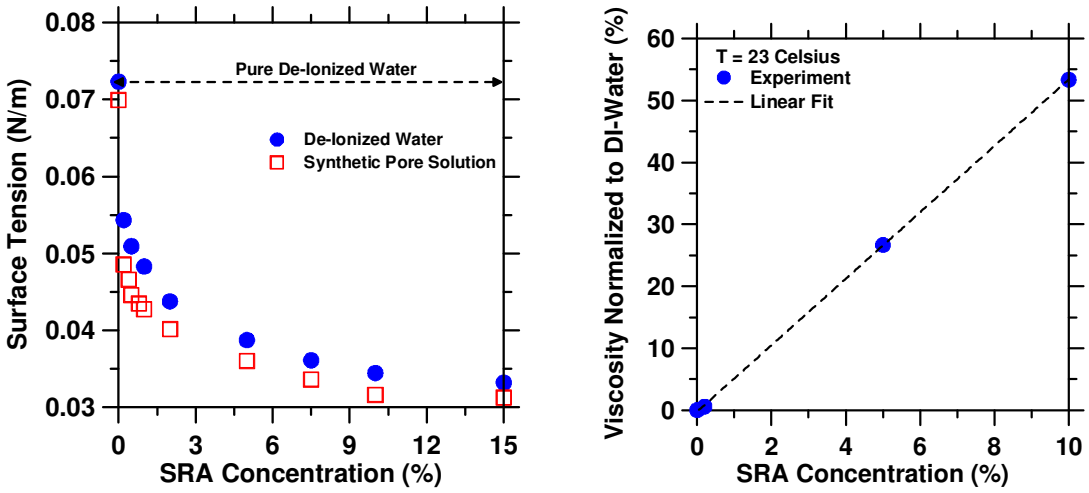

Figure 3: (a) Surface tension as a function of SRA concentration for DI-Water and synthetic pore solutions and (b) Viscosity increase as a function of SRA Concentration for DI-Water solutions

265 **7.2. Moisture Ingress Profiles Assessment Using X-Ray Absorption**

266

267 Figure 4 shows the time dependent moisture penetration profiles, for the plain and 5 % SRA
268 mixtures at 10 % hydration. In the figure, a ratio of x-ray intensity (transmitted) less than one
269 indicates a region where water has penetrated from the top surface (depth = 0), while a value
270 near 1.0 indicates a dry (original) region. It is seen that while the rate of moisture movement
271 (depth of penetration) is rapid in the plain mixture (Figure 4(a)), the rate of penetration is
272 significantly reduced in the SRA system, with approximately half the extent of penetration being
273 achieved in this system over the same time interval (Figure 4(b)).

274

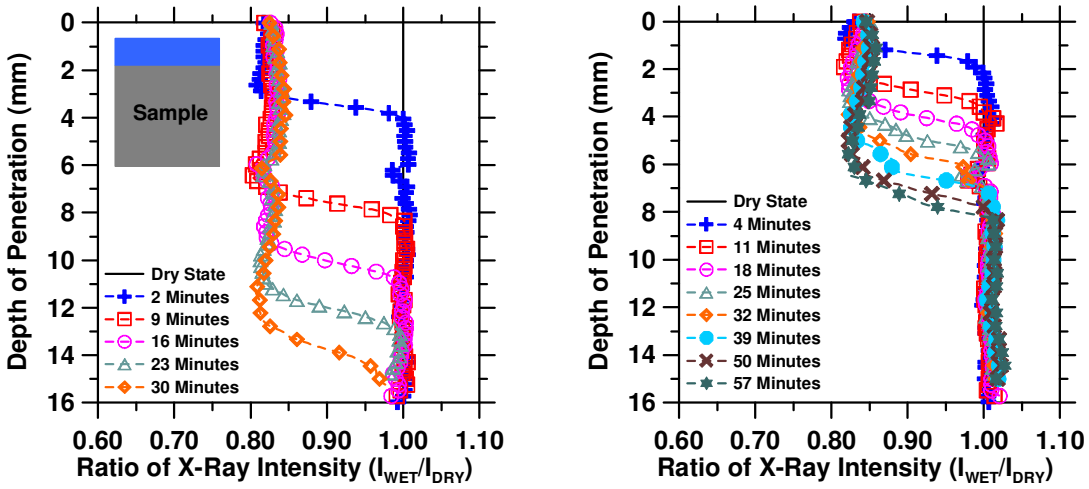

275

276 *(a)* *(b)*

277

278 Figure 4: The measured moisture ingress profiles as a function of x-ray intensity ratio at 10 %
279 hydration for: (a) a plain paste (*w/c* = 0.30) and (b) a paste containing a shrinkage-reducing
280 admixture (*w/c* = 0.30 + 5 % SRA)

281

8.0. Discussion of Experimental Results

8.1. The Influence of Surface Tension and Fluid Viscosity on Sorption: Experimental Observations and Theoretical Modeling

It is common to consider the parameter sorptivity (the rate of water absorption) to describe the moisture sorption behavior of a porous material [36]. The sorptivity is determined from the slope of the plot of volume of water absorbed as a function of the square root of the time from ponding, or in the case of spatially sensitive studies from a plot of the depth of penetration of water as a function of the square root of the time from ponding. Since water absorption is a process driven by capillary suction, the reduction in surface tension (and capillary pressure, Figure 5(a)), and the increase in viscosity effected by addition of an SRA would have significant implications on the sorption behavior of the system.

Measurements of sorptivity require fulfillment of certain considerations to be valid including; (a) a uniform initial water content, (b) one-dimensional flow and an unlimited supply of water at the ponding surface, (c) a homogenous material and (d) a material which is structurally and chemically unaltered by the infiltration of water [36]. While, conditions (a) to (c) are easily validated for cementitious materials, (d) presents difficulties especially in the case of early-age testing when a large proportion of unhydrated cement exists in the system. To minimize microstructural changes (and changes induced in the permeability and capillary suction forces due to pore refinement) and the 'sorptivity anomaly' induced due to continuing hydration, moisture ingress studies in this project were performed for a duration of only one hour [36].

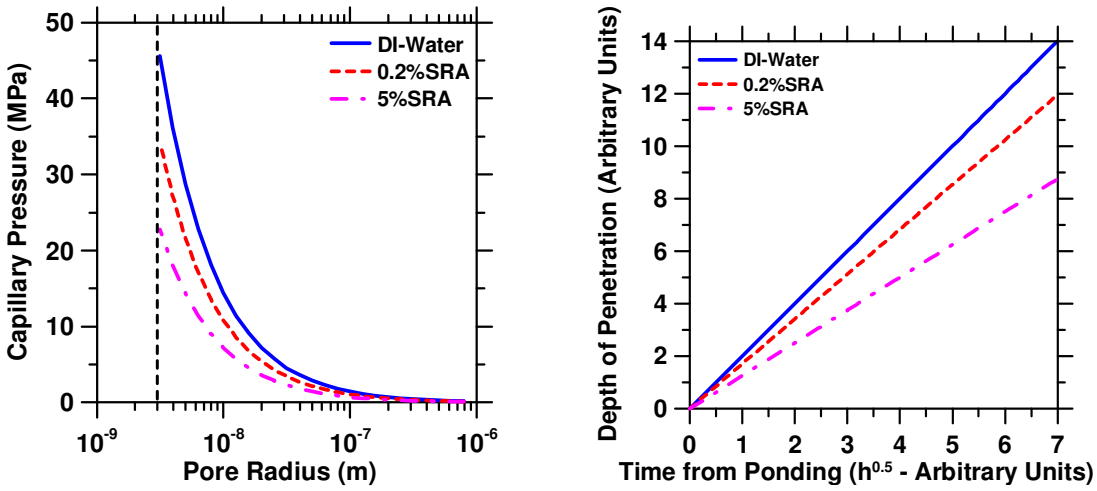

(a) *(b)*

Figure 5: (a) The capillary pressure as a function of the pore radius computed using the Young-Laplace equation. The dashed line indicates the thermodynamic stability limit of the liquid-vapor meniscus [37,38,39,40,41] and (b) The theoretical water sorption profiles for solutions containing different concentrations of a SRA computed using Kehlam's Formulation [47,48]

The reduction in surface tension and the increase in pore-fluid viscosity effected by addition of an SRA would exert a considerable influence on the sorptivity and water-absorption behavior of materials dosed with a shrinkage reducing admixture [36,42,43,44,45,46,47]. To comprehensively evaluate changes in water absorption induced by addition of a shrinkage reducing admixture, experimental observations of moisture ingress (Figure 4) were complemented by theoretical modeling of water absorption using a formulation developed by Kelham (Equation 7) [47,48].

$$x(t_t) = \sqrt{\frac{4 \cdot k \cdot \gamma \cdot \cos(\theta) \cdot t_t}{\phi \cdot \mu \cdot r}} \qquad \text{Equation (7)}$$

where: $x(t)$ is the depth of penetration (m) at any time t_t (s), k is the intrinsic permeability of the material (m^2), γ (N/m) is the surface tension of fluid, θ is the liquid-solid contact angle (radians), Φ is the porosity of the material (fraction), μ is the viscosity of the fluid (kg/(m·s)) and r (m) is the radius of the pore (capillary). In this study, the liquid-solid contact angles were determined using a linear interpolation of values reported previously for 0 % and 10 % SRA solutions (7° and 28° respectively) [42].

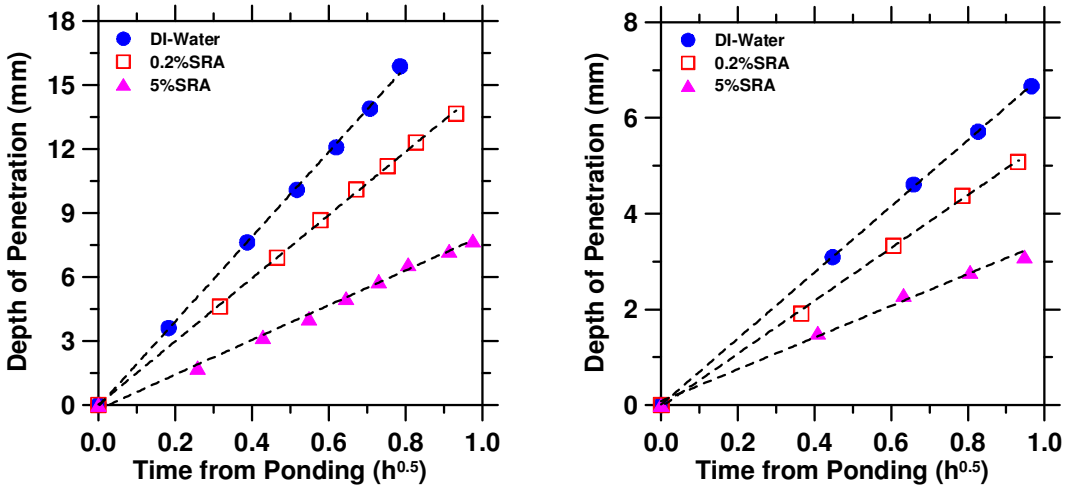

Figure 6: The measured depth of penetration and the sorption coefficients evaluated for cement paste mixtures at: (a) 10 % hydration and (b) 47 % hydration

Table 2: Experimentally Measured and Theoretically Modeled Sorption Coefficients

Cement Paste Mixture	Scaled Experimental Coefficient		Scaled Theoretical Coefficient
	10 % Hydration	47 % Hydration	
***w/c* = 0.30**	1.00	1.00	1.00
***w/c* = 0.30 + 0.2 % SRA**	0.75	0.79	0.84
***w/c* = 0.30 + 5 % SRA**	0.45	0.49	0.61

Considering each paste mixture displays a similar pore structure at an equivalent degree of hydration, we can assume similar values of porosity and intrinsic permeability for these systems [30,49]. Further, considering a ratio of surface tension values of 1.00:0.75:0.53 (Figure 3(a)), and a ratio of fluid viscosities values of 1.00:1.01:1.27 [47,48] (Figure 3(b)) for pure water, 0.2 % and 5 % SRA solutions, the depth of penetration (arbitrary units) and the sorptivity (slope of the depth of penetration versus square root of time curve) can be modeled for each mixture evaluated in this project. The results of this analysis are described in Figure 5(b) and summarized in Table 2. The sorptivity values determined from theoretical modeling for each of these systems, pure water, 0.2 % SRA and 5 % SRA scale as 1.00:0.84:0.61 respectively. It is seen, the ratio of sorptivity's determined from theoretical modeling are in good agreement with the scaled values of sorptivity determined from experimental measurements (Table 2). The difference observed in the measured and modeled sorption coefficients may be attributed to the change in the SRA concentration as a function of specimen maturity (hydration) and increasing water absorption into the pore structure, which would exert a larger influence on the results with increasing SRA concentration (as evidenced).

It is noted that a linear fit of the experimental water absorption measurements display's a small non-zero intercept. This may be explained due to air-trapping and surface and edge effects in the

specimen [36]. The agreement between experimental and modeling approaches is significant in that, for measurements performed over a short time scale, it would allow estimation of the sorptivity for various mixtures and ingressing fluids, permitting determination of the fluid saturation level in the material. While in this study, the ingressing fluid was DI water and the SRA was supplied from within the cement paste, previous measurements of the ingress of both DI water and a 10 % SRA solution into hardened cement paste specimens (containing no SRA) have also supported the validity of the $\sqrt{(\gamma/\mu)}$ scaling of sorption coefficients [50].

The results of theoretical modeling and experimental observations of water sorption illustrate an important point; even upon cycles of drying and wetting, the SRA is observed to persist in the material and is capable of altering the moisture absorption and shrinkage behavior [44,51,64]. It is hypothesized that upon drying, the SRA is adsorbed/absorbed onto the pore walls and maintains this state until a cycle of rewetting is experienced, when the SRA goes back into the pore solution. This has significant implications on the durability performance of materials containing an SRA and will be discussed further in Section 8.3.

8.2. The Boltzmann-Matano Approach for Assessment of the Moisture Diffusivity

One-dimensional moisture diffusion in a unsaturated porous medium can be described in the case of single-phase, isothermal moisture transport as shown in Equation (8) [36,52]:

$$\frac{\partial w}{\partial t} = \frac{\partial}{\partial x} \cdot \left(D(w) \cdot \frac{\partial w}{\partial x} \right) \qquad \text{Equation (8)}$$

where: w is the moisture content (fraction), $D(w)$ is the moisture content dependent liquid moisture diffusivity (units of m^2/s) and x and t denote variables for spatial position and time. In

the case of moisture transport in a semi-infinite, isotropic, homogenous medium that has a uniform initial moisture w_i and a constant (or final) moisture content w_f at the boundary furthest from the wetting end, the diffusivity function has been determined to have a unique, closed-form solution using a procedure known as the Boltzmann transformation (Equation 9) [36,53,54,55,56].

$$D(w) = -\frac{1}{2} \cdot \left(\left(\frac{\partial \lambda}{\partial w} \right)_w \right) \cdot \int_{w_i}^{w_f} \lambda \cdot dw \qquad \text{Equation (9)}$$

where: λ is the Boltzmann variable (mm/h$^{0.5}$). A primary consideration for the validity of the transformation dictates that the wetting front should not reach the bottom of the specimen (the region having fixed moisture content). For measurements which satisfy the criteria of the Boltzmann transformation, when the wetting profiles are represented as a function of the Boltzmann variable, λ, all the experimental measurements should collapse onto a single master curve, known as the characteristic moisture profile which indicates the moisture content (or in this case the normalized x-ray intensity) as a function of the Boltzmann variable (Equation 10).

$$\lambda = \frac{x}{\sqrt{t}} \qquad \text{Equation (10)}$$

The characteristic moisture profiles for two cement paste mixtures (*w/c* = 0.30 and *w/c* = 0.30 + 5 % SRA) at 10 % hydration are illustrated in Figure 7 [36]. Figure 7 shows moisture penetration profiles which have been subjected to the Boltzmann transformation. The fitted Boltzmann-Matano curve of the experimental ingress profiles is seen to provide a good representation of the measured moisture ingress profiles within a small region of scatter (Figure 7) [64].

The characteristic curve shows four distinct stages which corresponds to regions having four different moisture contents in the specimen (Figure 7(a)), Stage-I is the surface zone, closest to the wetting water and shows the highest moisture content (lowest intensity) corresponding to

saturation of the specimen surface [26]. Complete saturation at the surface is achieved only when the air entrapped in the pore structure diffuses out. It has been noted by previous researchers that this is a very slow process which can continue for months [36]. It is important to indicate that while the Boltzmann transformation has been demonstrated to reliably replicate the experimental response, conceptually, the application of such a transformation is not completely accurate over every region of the characteristic moisture profile. The closed-form solution of the diffusion approach used in the Boltzmann transform is valid only in the case of single phase diffusion. In the surface zone (stage-I), there exists two-phase diffusion, namely water diffusing into the cement paste and air trapped in the microstructure diffusing out. However, it is noticed (Figure 7) in spite of the violation of the single-phase diffusion approach, the Boltzmann transformation reliably replicates the experimental response, demonstrating from practical considerations that the single-phase diffusion approach may be considered valid, given the small contribution of air diffusion at short time scales [36].

Stage-II is a region of almost uniform moisture content (constant intensity) and corresponds to a diffuse-moisture zone preceding the wetting front. The movement of moisture in the diffuse zone is driven by capillary forces which suck moisture into the sample. Issues of air-trapping in the diffuse and wetting zones are crucial, with saturation not being achieved until all the entrapped air is able to diffuse out.

Stage-III corresponds to the wetting front that penetrates progressively deeper into the specimen with increasing time. This region shows the largest variability in moisture content (intensity), as a function of increasing depth (and Boltzmann variable).

427 Stage IV corresponds to the region having uniform moisture content (w_f) throughout the course
428 of the imbibition experiment which satisfies the semi-infinite medium diffusion criteria of the
429 Boltzmann-Matano approach.

430

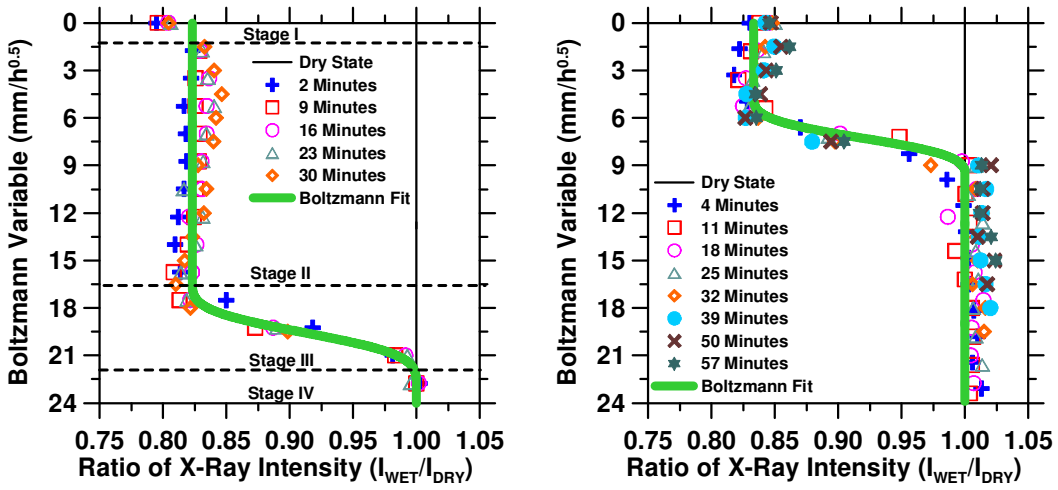

431

432 *(a)* *(b)*

433

434 Figure 7: The Boltzmann transformed ingress profiles illustrating the Boltzmann variable as a
435 function of x-ray intensity for specimens at 10 % hydration for: (a) a plain paste (*w/c* = 0.30) and
436 (b) a paste containing a SRA (*w/c* = 0.30 + 5 % SRA)

437

438 **8.3. The Influence of SRA Addition and Specimen Maturity on the Moisture Diffusivity**

439

440 Isothermal moisture transport in porous materials can be adequately represented using a non-
441 linear diffusion equation (Equation 8) [[36]]. In Equation 8, all mechanisms of moisture movement
442 distribution and transfer (liquid and vapor) are represented by a single moisture diffusivity, *D(w)*,
443 which is dependent upon the local moisture content of the material. The moisture diffusivity

increases with increasing moisture content, showing a dramatic increase at saturation. When the diffusivity is combined with the initial and boundary conditions of the element under evaluation, the moisture transfer performance of building materials can be comprehensively predicted [57,61].

The moisture diffusivity of a porous material can be calculated from transient moisture transfer measurements, shown in Figure 5 [58,59]. The Boltzmann-Matano approach can then be used to yield the characteristic moisture profile shown in Figure 7 [36,60]. Traditionally, the moisture content dependent moisture diffusivity (for absorption, imbibition or infiltration type processes) for concretes has been represented as an exponential function (Equation 11) [36,59,61,62,63].

$$D(w) = D_0 \cdot \exp(\beta \cdot w) \qquad \text{Equation (11)}$$

where: D_0 and β are constants which depend upon the properties of the material. In this work, the exponential function has been fit over the linear range of the moisture diffusivity function due to the difficulties associated with accurately describing the moisture diffusivity at very low and very high moisture content levels.

Figure 8 shows the moisture diffusivity of cement pastes at 10 % and 47 % hydration computed using an averaging and curve-fitting procedure and Equation 9 [64]. It is seen (Figure 8(a)) that pastes containing SRA (0.2 % and 5 %) exhibit lower moisture diffusivity D_0 and higher β values as compared to the plain cement paste (Table 3). This behavior can be explained by the reduction in surface tension of the pore fluid and increase in fluid viscosity, induced by addition of the admixture which reduces capillary suction (and absorption) and the tendency of the material to transmit fluids due to capillarity (refer section 8.1). The point at which the diffusivity dramatically increases corresponds to the surface zone, closest to the water source, where

467 saturation is achieved. Further, the assumption of plain and SRA mixtures exhibiting similar
468 porosities is validated as the moisture diffusivity dramatically increases at similar moisture
469 contents, corresponding to porosity saturation.

470

471 **Table 3: Moisture Diffusivity Parameters for Cement Pastes at 10 % and 47 % Hydration**

472

Moisture Diffusivity Parameters	10 % Hydration		47 % Hydration	
	D_0 (m^2/s)	β	D_0 (m^2/s)	β
***w/c* = 0.30**	1.36E-09	8.13	7.23E-10	8.48
***w/c* = 0.30 + 0.2 % SRA**	4.20E-10	9.62	3.63E-10	9.72
***w/c* = 0.30 + 5 % SRA**	3.96E-10	9.99	8.95E-11	10.50

473

474 In addition to the change in surface tension, pore structure refinement with increasing hydration
475 would also influence the moisture diffusivity of the material. This influence is evident in Table 3
476 which shows a reduction in the moisture diffusivity, D_0, with increasing hydration. This is
477 reasonable considering that a less porous microstructure would exert a larger resistance to the
478 movement of moisture. Further, it is interesting to note the β parameter increases with increasing
479 maturity (structure densification), and exhibits an opposing trend to the D_0 value (which
480 decreases with increasing hydration). The value of the β calculated compares well with the value
481 (β = 4-9) reported in the literature for mature building materials [36,46,57,61,62].

482

483 The change in the moisture diffusivity achieved by addition of a shrinkage reducing admixture
484 has powerful implications on curing, freeze-thaw performance and ion-migration in these
485 mixtures. The reduced moisture diffusivity and the sorptivity of SRA mixtures suggests the depth

of fluid penetration in these mixtures at short-time scales would be less than in plain cement mixtures. This may imply less water absorption during curing in these mixtures over short curing durations. The reduced sorptivity and moisture diffusivity could indicate a longer time to saturation which may enhance the performance of these mixtures when subjected to freeze-thaw loadings [65]. Further, the decreased moisture diffusivity may indicate better durability performance in concretes containing a SRA due to decreased moisture (and consequently aggressive ion) migration in these materials [43].

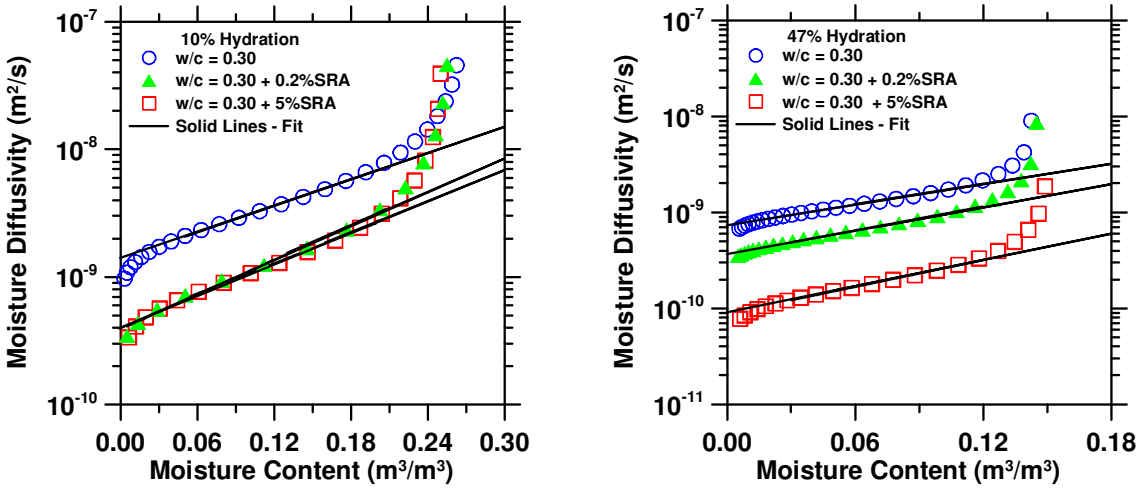

(a) *(b)*

Figure 8: The moisture content dependent moisture diffusivity as a function of the moisture content for cement pastes at: (a) 10 % hydration and (b) 47 % hydration

9.0. Summary and Conclusions

In conclusion, this paper has described the water absorption behavior of cement pastes containing various concentrations of a shrinkage reducing admixture. X-ray absorption measurements were used to provide high resolution spatial information on the movement and depth of penetration of moisture. The Boltzmann-Matano concentration dependent diffusion approach was used to profile the characteristic moisture curve, which enabled determination of the wetting moisture diffusivity. It was observed that the addition of an SRA results in a reduction in surface tension and an increase in fluid viscosity. The addition of an SRA reduces the sorptivity and wetting moisture diffusivity. Further, the reduction in the sorptivity, measured for mixtures containing an SRA, compared well with theoretical modeling of the sorption coefficient. The sorptivity and moisture diffusivity were both observed to decrease with increasing maturity and pore structure refinement.

The outcome of this investigation has powerful implications as it relates to the durability and moisture transfer performance of concrete mixtures containing surface-tension and viscosity altering admixtures. The reduction in moisture diffusivity effected by addition of an SRA influences the durability performance of cementitious materials, due to allied considerations of curing (reduction in the depth of curing water) and ion diffusivity (reduced chloride and deleterious ion migration), and may suggest improved freeze-thaw (decreased saturation levels) performance of the system. This assumes significance in the context of predicting the service life of these materials, and substantiates the need for determining appropriate input parameters for computer models which aim to make such predictions for concrete structures.

526 **Acknowledgements**

527

528 This work was conducted in the Building and Fire Research Laboratory (BFRL) at the National
529 Institute of Standards and Technology (NIST) and the Materials Sensing and Characterization
530 Laboratory at Purdue University using the x-ray absorption facility made possible through a
531 grant to the fourth author for the development of a Materials and Moisture Characterization
532 Laboratory. As such, the authors would like to acknowledge the support which has made these
533 laboratories and this research possible. The contents of this paper reflect the views of the authors,
534 who are responsible for the accuracy of the data presented. The authors would also like to
535 acknowledge Edward Garboczi (NIST) and Nicos Martys (NIST) for their review of this paper.

536

537 **References**

538

[1] Weiss, W. J., and Berke, N. S., 'Shrinkage reducing admixtures', in Early Age Cracking in Cementitious Systems, RILEM State of the Art Report, Edited: Bentur, A., (2002).

[2] Ai, H., and Young, J. F., 'Mechanisms of Shrinkage Reduction Using a Chemical Admixture', Proceedings of the 10th International Congress on the Chemistry of Cement, Edited: Justnes, H., Gothenburg, Sweden, 3, (1997).

[3] Shoya, M., and Sugita M., "Application of Special Admixture to Reduce Shrinkage Cracking of Air Dried Concrete," Hachinohe Institute of Technology, Hachinohe, Japan, (1990).

[4] Shah, S. P., and Weiss, W. J., 'High Strength Concrete: Strength, Permeability, and Cracking', Proceedings of the PCI/FHWA International Symposium on High Performance Concrete, Orlando, Florida, pp. 331-340, (2000).

[5] Weiss, W. J., Schissel, A., Yang, W., and Shah, S. P, 'Shrinkage Cracking Potential, Permeability, and Strength, for HPC: Influence of w/c, Silica Fume, Latex, and Shrinkage Reducing Admixtures', International Symposium on High Performance and Reactive Powder Concrete, Sherbrooke, Canada, pp. 349-364, (1998).

[6] Bentz, D.P., Geiker, M.R., and Hansen, K.H., 'Shrinkage-Reducing Admixtures (SRAs) and Early Age Desiccation in Cement Pastes and Mortars', Cement and Concrete Research, 31(7), pp. 1075-1085, (2001).

[7] Shah, S.P., Karaguler, M.E., and Sarigaphuti, M., 'Effects of shrinkage reducing admixture on restrained shrinkage cracking of concrete', ACI Materials Journal, 89(3), pp. 88-90, (1992).

[8] Ribeiro, A., Carrajola, A., Goncalves, A., and Branco, F., 'Effectiveness of shrinkage reducing admixtures on cracking of mortar specimens', Proceedings of the RILEM-JCI Sem. on Concrete Durability and Service Life Planning' ConcreteLife'06, 2006, Ein-Bokek, Israel, (2006).

[9] See, H. T., Attiogbe, E. K., and Miltenberger, M. A., 'Shrinkage Cracking Characteristics of Concrete Using Ring Specimens', ACI Materials Journal, 100(3), pp. 239–245, (2003).

[10] D'Ambrosia, M.D., Altoubat, S., Park, C., and Lange, D. A., 'Early-Age Tensile Creep and Shrinkage of Concrete with Shrinkage Reducing Admixtures', Creep, Shrinkage, and Durability Mechanics of Concrete and Other Quasi-Brittle Materials, Editors: Ulm, F. J., Bazant, Z. P., and Wittmann, F. H., Elsevier, Cambridge MA, pp. 645-651, (2001).

[11] Schissel, A., Weiss, W. J., Shane, J. D., Berke, N. S., Mason, T.O., and Shah, S. P., 'Assessing the Moisture Profile of Drying Concrete Using Impedance Spectroscopy', Concrete Science and Engineering, 2, pp. 106-116, (2000).

[12] Berke, N. S., Dallaire, M. C., Hicks, M. C., and Kerkar, A., 'New Developments in Shrinkage-Reducing Admixtures, Superplasticizers and Other Chemical Admixtures in Concrete', Proceedings Fifth CANMET/ACI International Conference, Rome, Italy, (1997).

[13] Cope, B. L., and Ramey, G.E., 'Reducing Drying Shrinkage of Bridge Deck Concrete', Concrete International, 23(8), pp. 76-82, (2001).

[14] Schemmel, J. J., Ray, J. C., and Kuss, M. L., 'Impact of Shrinkage Reducing Admixture on Properties and Performance of Bridge Deck Concrete', High-Performance Concrete Research to Practice, ACI SP-189, American Concrete Institute, Michigan, pp. 367–386, (1999).

[15] Bissonnette, B., 'Personal Communication', November, (2006).

[16] Berke, N. S., and Weiss, W. J., 'Personal Communication', (2005).

[17] Weiss, W. J., 'Unpublished Results', Purdue University, West Lafayette, USA, (2004).

[18] Winslow, D.N., Cohen, M.D., Bentz, D.P., Snyder, K.A., Garboczi, E.J., 'Percolation and Pore Structure in Mortars and Concrete', Cement and Concrete. Research, 24(1), pp. 25-37, (1994).

[19] Sant, G., Lura, P., and Weiss, W.J., 'Measurement of Volume Change in Cementitious Materials at Early Ages: Review of Testing Protocols and Interpretation of Results', The Transportation Research Record, 1979, (2006).

[20] GNI, www.gni.dk, October 30, (2007).

[21] Nielsen, G. G., 'X-Ray CT System – Users Manual', GNI/XRAS/UM.003, 3, June 17, (2007).

[22] Paradis, F., and Weiss, W. J., 'Using X-Ray Tomography to Image Cracks in Cement Pastes', International Conference on High-Performance Fiber-Reinforced Concrete Composites (HPFRCC), Stuttgart, Germany, (2007).

[23] Wagenaart, D. J., DiBianca, A. F., Tenney, C. R., and Fritsch, D., 'Space charge effects in a kinestatic charge detector', Physical Medicine and Biology, Vol. 36 (1), pp. 61-76, (1991).

[24] Als-Nielsen, J., and McMorrow, D., 'Fundamentals of Modern X-Ray Physics', John Wiley and Sons Limited, Chichester, United Kingdom, (2006).

[25] Sant, G., and Weiss, W. J., 'The Use of X-Ray Absorption for Assessing Moisture Movement in Cementitious Materials' submitted to the Journal of Cement and Concrete Composites, (2008).

[26] Roels, S and Carmeliet, J., 'Analysis of moisture flow in porous materials using microfocus X-ray radiography', International Journal of Heat and Mass Transfer, 49, pp. 4762–4772, (2006).

[27] Mouze, D., 'X-ray microradiography', in: S. Amelincks, D. Van Dyck, J. Van Landuyt, G. Van Tendeloo (Eds.), Handbook of Microscopy I, VCH, Weinheim, pp. 130–147, (1996).

[28] Adamson, A. W., 'Physical Chemistry of Surfaces', Wiley, pp. 777, (1990).

[29] Weast, R. C., Astle, M. J., and Beyer, W. H., ' CRC Handbook of Chemistry and Physics', 88th Edition, CRC Press, pp. 2640, (2007).

[30] Sant, G., 'Examining Volume Changes, Stress Development and Cracking in Cement-Based Materials', Master's Thesis, Purdue University, West Lafayette, USA, (2007).

[31] Sant, G., Rajabipour, F., Lura, P., and Weiss, W. J., 'Examining Time-Zero and Early-Age Expansions in Pastes Containing Shrinkage Reducing Admixtures (SRAs)', 2nd RILEM Symposium on Advances in Concrete through Science and Engineering, Canada, (2006).

[32] Sant, G., Bentz, D. P., and Weiss, W. J., 'Examining the Connectivity of Moisture in Cementitious Materials at Early Ages', prepared for submission to Cement and Concrete Research, April, (2008).

[33] Pease, B. J., Shah, H. R., Weiss, W. J., Shrinkage behavior and residual stress development in mortar containing shrinkage reducing admixture (SRA's), Shrinkage and creep of concrete, ACI SP-227, Special Publication on Concrete Admixtures, Farmington Hills, Michigan, (2005).

[34] Control of Shrinkage, Early-Age Cracking; Causes, Measurement, and Mitigation, ACI Committee 231 Report (Under Development), American Concrete Institute, Farmington Hills, Michigan (2007) Chapter 4.0, (2007).

[35] Rajabipour, F., Sant, G., and Weiss, W. J., 'Interactions between Shrinkage Reducing Admixtures (SRAs) and Cement Paste's Pore Solution', Cement and Concrete Research, Article in Press (available online), doi:10.1016/j.cemconres.2007.12.005, (2008).

[36] Hall, C., and Hoff, W. D., 'Water-Transport in Brick, Stone and Concrete', Spon Press, London United Kingdom, (2002).

[37] Christenson, H.K., 'Capillary Condensation in Systems of Immiscible Liquids', Journal of Colloid and Interface Science, 104 (1), (1985).

[38] Fischer, L. and Israelachivili, J., 'Experimental Studies on the Applicability of the Kelvin Equation to Highly Curved Concave Menisci', Jour. of Colloid and Interface Sci., 80 (2), (1981).

[39] Fischer, L. and Israelachivili, J., 'Direct Measurement of the Effect of Meniscus Forces on Adhesion: A Study of the Applicability of Macroscopic Thermodynamics to Microscopic Liquid Interfaces', Journal of Colloids and Surfaces, 3, pp. 303-319, (1981).

[40] Digilov, R., 'Kelvin Equation for Meniscuses of Nanosize Dimensions', Langmuir, 16, pp. 1424-1427, (2000).

[41] Weiss, W. J., Lura, P., Rajabipour, F., and Sant, G., 'Performance of Shrinkage Reducing Admixtures at Different Humidities and at Early-Ages' accepted by ACI Materials Journal, (2008).

[42] Bentz, D.P., 'Influence of Shrinkage-Reducing Admixtures on Early-Age Properties of Cement Pastes', Journal of Advanced Concrete Technology, 4(3), pp. 423-429, (2006).

[43] Bentz, D. P., Snyder, K. A., Cass, L. C., and Peltz, M. A., 'Doubling the Service Life of Concrete I: Reducing Ion Mobility Using Nanoscale Viscosity Modifiers', accepted by Cement and Concrete Composites, (2008).

[44] Pease, B.J., 'The Role of Shrinkage Reducing Admixtures on Shrinkage, Stress Development, and Cracking', MSCE Thesis, Purdue University, West Lafayette, Indiana, (2005).

[45] Rajabipour, F., 'Insitu Electrical Sensing and Material Health Monitoring in Concrete Structures', PhD Dissertation, Purdue University, West Lafayette, IN, USA, (2006).

[46] 'Penetration and Permeability of Concrete – Barriers to Organic and Contaminating Liquids', RILEM Report 16, Edited: Reinhardt, H. W., E and FN Spon, (1997).

[47] Weiss, W. J., 'Prediction of Early-Age Shrinkage Cracking in Concrete', PhD Dissertation, Northwestern University, Evanston, USA, (1999).

[48] Kelham, M., 'A water absorption test for concrete', Magazine of Concrete Research, 40, pp. 143, (1998).

[49] Sant, G., and Weiss, W. J., 'Unpublished Results', Purdue University, USA, Dec, (2006).

[50] Bentz, D.P., 'Influence of Shrinkage-Reducing Admixtures on the Early-Age Properties of Cement Pastes', presentation at the ACI Fall convention, Denver, USA, (2006).

[51] Weiss, W. J., 'Unpublished Results', Purdue University, West Lafayette, USA, (2008).

[52] Richards, L. A., 'Capillary Conduction of Liquids through Porous Media', Physics, 1, (1931).

[53] Crank, J., 'The Mathematics of Diffusion', Oxford, Clarendon Press, United Kingdom, (1975).

[54] Besien, T. V., Roels, S., and Carmeliet, J., 'Experimental Determination of the Moisture Diffusivity of Porous Building Materials using X-Ray radiography', 6th Nordic Symposium on Building Physics, (2002).

[55] Matano, C., 'On the relation between diffusion coefficients and concentrations of solid metals (the nickel-copper system)', The Japanese Journal of Physics, 8, pp. 109-113, (1932-33).

[56] Bruce, R. R., and Klute, A., 'The measurement of soil-moisture diffusivity', Proceedings of the Soil Science Society of America, 20, pp. 458-462, (1956).

[57] Lockington, D., Parlange, J. Y., and Dux, P., 'Sorptivity and the Estimation of Water Penetration into Concrete', Materials and Structures, 32, pp. 342-347, (1999).

[58] Carmeliet, J., Adan, O., Brocken, H., Cerny, R., Hall, C., Hens, H., Kumaran, K., Pavlik, Z., Pel, L., Plagge, R. and Roels, S., 'Determination of the Liquid Water Diffusivity from Transient Moisture Transfer Experiments', Journal of Thermal Envelope and Building Science, 27(4), pp. 277–305, (2003).

[59] Pel, L., 'Moisture Transport in Porous Building Materials', PhD Thesis, Eindhoven University of Technology, the Netherlands, (1995).

[60] Pel, L., Brocken, H., Kopinga, K., 'Determination of moisture diffusivity in porous media using moisture concentration profiles', International Journal of Heat and Mass Transfer, 39 (6), pp.1273–1280, (1996).

[61] Leech, C., Lockington, D., and Dux, P., 'Unsaturated Diffusivity Functions for Concrete Derived from NMR Images', Materials and Structures, 36, pp. 413-418, (2003).

[62] Hall, C., 'Water Sorptivity of Mortars and Concretes – A Review', Magazine of Concrete Research, 41, pp. 51-61, (1989).

[63] Daian, J. F., 'Condensation and Isothermal Water Transfer in Cement Mortar – Part I – Pore Size Distribution, Equilibrium Water Condensation and Imbibition', Transport in Porous Media, 3, pp. 563-589, (1988).

[64] Sant, G., 'Moisture Movement, Distribution and Transfer in Cement Based Materials', PhD Dissertation (In Development), Purdue University, West Lafayette, IN, USA, (2009).

[65] Fagerlund, G., 'Critical Degrees of Saturation at Freezing of Porous and Brittle Materials', (In Swedish) Division of Building Technology, Lund Institute of Technology, Report Number 34, Lund, Sweden, (1973).